Supramolecular structure of helical ribbons self-assembled from a β-sheet peptide

Wonmuk Hwang
Center for Biomedical Engineering and Division of Biological Engineering, Massachusetts Institute of Technology, Cambridge, Massachusetts 02139

Davide M. Marini and Roger D. Kamm[a)]
Division of Biological Engineering and Department of Mechanical Engineering, Massachusetts Institute of Technology, Cambridge, Massachusetts 02139

Shuguang Zhang
Center for Biomedical Engineering, Massachusetts Institute of Technology, Cambridge, Massachusetts 02139

(Received 11 June 2002; accepted 4 October 2002)

We have investigated the supramolecular structure of helical ribbons formed during self-assembly of a β-sheet peptide using computer simulation. We tested a wide range of molecular packing geometries consistent with the experimental dimensions to identify the most stable structure, and then systematically changed the helical geometry to investigate its energy landscape. The effect of pH was incorporated by scaling the amount of charge on the side chains based on the electrostatic double layer theory. Our results suggest that these left-handed helical ribbons are comprised of a double β-sheet and that the experimentally measured dimensions correspond to a local energy minimum. Side chain interactions are found to be critical in determining the stability and curvature of the helix. Our approach has general applicability to the study of self-assembled nanostructures from β-sheet peptides where high resolution data are not yet available. © *2003 American Institute of Physics.* [DOI: 10.1063/1.1524618]

I. INTRODUCTION

Beta-sheet peptides have recently drawn great interest because of their potential in biomedical applications. Under appropriate conditions, they self-assemble to form networks of fibers with diameters on the order of nanometers.[1–3] Hydrogels made of these fibers show rheological properties that depend on solution pH[4] or on shear stress.[5] These hydrogels are currently used as three dimensional scaffolds for growing neurons[2] and cartilage.[6] Moreover, these fibers share many distinctive features with the amyloid fibrils found in protein conformational diseases and are therefore used as model systems to study the formation and structure of amyloids.[1,7–10]

The determination of the supramolecular architecture of β-sheet fibers has been difficult, even for the most widely studied amyloid fibrils. Since they do not form single crystals, x-ray diffraction could only reveal rough features of the β-sheet.[7] Due to their large aggregate size, solution-phase nuclear magnetic resonance (NMR) is also unsuitable. Fourier transform infrared spectroscopy (FTIR) and especially solid state NMR have been more successful in providing useful information about the molecular packing.[11–15] However, even the basic issue of β-strand orientation, parallel or anti-parallel, has not yet been completely resolved.

Recent studies have shown that β-sheet fibers are usually formed through various intermediates such as helical ribbons,[3,16] globular aggregates,[8] or toroids.[17] The structure and properties of the intermediates are thus important in understanding the process of self-assembly. Moreover, in the case of amyloidosis, the intermediate rather than the final fibril may be the pathogenic species.[16,18,19]

Here we investigate the helical ribbon intermediates formed during self-assembly of the β-sheet peptide KFE8 (amino acid sequence: FKFEFKFE, Fig. 1).[3] Helical ribbons are also found in other self-assembling systems, such as surfactants,[20] lipids,[21–23] chlorophelols,[24] liquid crystalline polymers,[25] and certain disk-shaped molecules.[26] The dimensions of these helices vary from nanometers to microns and they are usually formed through noncovalent bonding between constituent monomers. They also show interesting dynamical behaviors such as transition between distinct helical pitches[22] and supercoiling.[26–28]

Current theories of self-assembled helical ribbons are mostly based on a continuum description, using coarse-grained quantities like interfacial energies or elastic moduli.[22,27,29,30] Although they have been successful in explaining some of the observed phenomena, a description at the atomic level is necessary in order to predict properties that depend on the molecular details and to assist in further development of the continuum theory.

Here we use a computational approach to investigate at the atomic level the supramolecular structure of the helical ribbons formed by KFE8. Our method consists of constructing a wide variety of molecular packing geometries that are consistent with the dimensions found experimentally. We evaluate each of them by molecular dynamics (MD) simulations to identify the most stable structure. We then vary the geometry of that stable structure to confirm that the experi-

[a)]Electronic mail: rdkamm@mit.edu

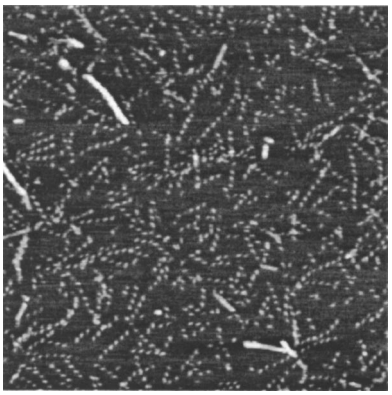

FIG. 1. Helical ribbon intermediates in the self-assembly of the β-sheet peptide KFE8 observed under atomic force microscopy (AFM) (Ref. 3). These structures appear minutes after dissolving the peptide in water and become solid fibers after a few hours. The image is 1 μm$\times$1 μm in size.

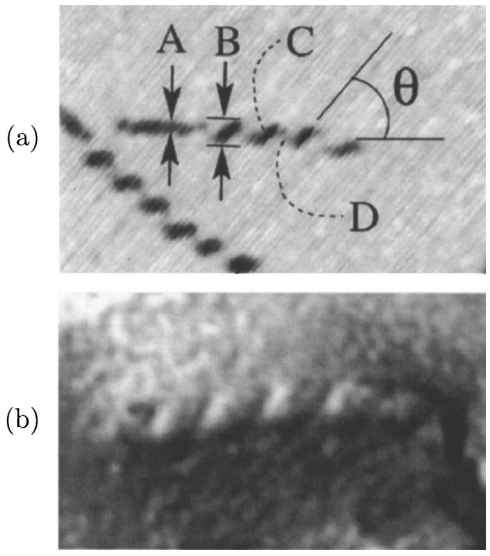

FIG. 3. (a) A magnified view of the AFM image, color inverted for visibility. Approximate dimensions measured from the image are the following: region A: 6.4 nm wide [W] and 2.1 nm high [H], B: 11 nm [W], C: 2.9 nm [H], and D: 3.4 nm [W], 0.9 nm[H]. The pitch angle θ is defined as shown. (b) A QFDE-TEM image of the helical ribbon (Ref. 3). Due to the platinum coat, the fature looks fatter. The above two images are not to the same scale.

mentally measured dimensions correspond to a local minimum in its energy landscape. Such an approach has general applicability to the analysis of other intermediate structures, such as toroids or globules where there is a relatively small number of possible packing geometries.

The paper is organized as follows. In Sec. II we explain the procedure of constructing β-sheets and helices from individual molecules. In Sec. III, the electrostatic double layer theory is applied to calculate surface charge densities of the helical ribbon in given electrolyte conditions. We explain our simulation method in Sec. IV and discuss the results in Sec. V. A summary and a discussion of future directions are given in Sec. VI.

II. HELIX CONSTRUCTION

Since self-assembly of β-sheet peptides occurs over a time scale longer than seconds, a simulation starting from dispersed monomers would be computationally prohibitive. Here we use the alternative approach of constructing the final helical structure and testing its stability. To do so, we relied on the tendency of KFE8 to form β-sheets, implied by its pattern of alternating hydrophobic–hydrophilic residues (Fig. 2),[31,32] and used this as the fundamental building block.

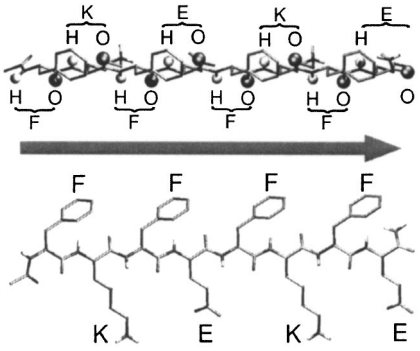

FIG. 2. Top and side views of KFE8. Lysine (K, Lys) and glutamic acid (E, Glu) are hydrophilic, while phenylalanine (F, Phe) is hydrophobic. The arrow symbolizes the peptide in β-strand conformation. The N and C termini are, respectively, acetylated and amidated. Backbone hydrogens and oxygens are emphasized as spheres in the top view. The size of one KFE8 molecule is approximately $3.1\times1.2\times0.4(\mathrm{nm}^3)$.

A. Dimensions of the helix

Structural information about the helical ribbon can be obtained from the measured dimensions in Fig. 3(a). When interpreting the data, the following two aspects of the AFM should be taken into account: Due to the finite size of the AFM tip (3–5 nm radius of curvature) the lateral dimensions tend to be overestimated. On the other hand, the attractive interaction between the sample and mica substrate and the presence of the background layer of monomers and smaller aggregates cause the vertical dimension to be underestimated.

With these considerations, and from the dimensions of a single KFE8 (Fig. 2), the region A in Fig. 3(a) is a single molecule wide. Its height is slightly less than twice the height of KFE8, suggesting that this region is a straightened double sheet. The cross section of the regions B and C has an elliptical shape, suggesting that the helical ribbon is vertically compressed due to the sample–substrate attraction. Region D seems to be partially buried in the background layer and the tip artifact is less pronounced in this region due to its low height, rendering its width close to one molecule. This supports the view that the helical ribbon is composed of a one-molecule wide tape.

While the above quantities suffer from over- or underestimations, the pitch of the helical ribbon and the pitch angle, defined as the angle between the axis of the helix and the contour line, can be measured without systematic error. An analysis of approximately 150 ribbons yielded a pitch h of 19.4 ± 1.3 nm and a pitch angle θ of $41.1\pm5.7°$. Assuming cylindrical geometry, the radius r of the helix can be obtained from the relation $r\simeq h\tan\theta/2\pi=2.69$ nm. Similar values were obtained from the quick-freeze–deep-etch trans-

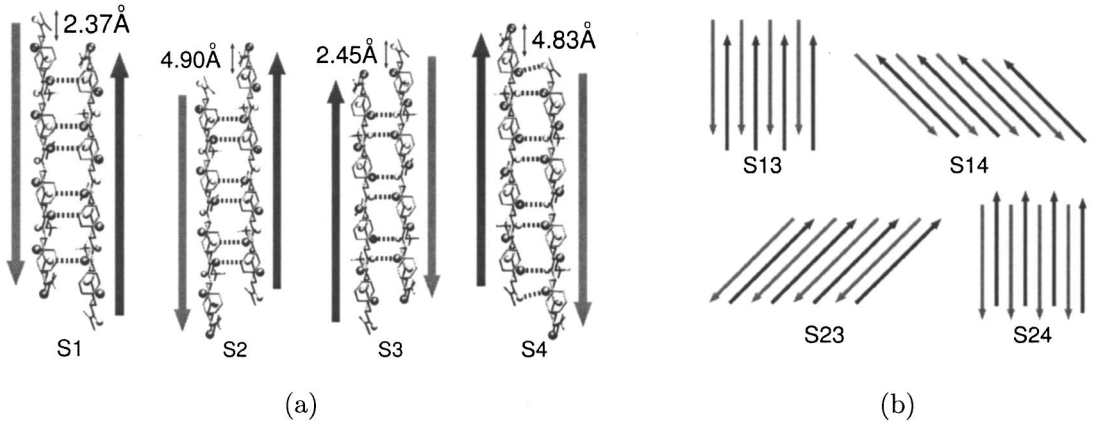

FIG. 4. (a) Hydrogen bonding patterns between adjacent peptides in an anti-parallel β-sheet. Phenyl rings point toward the reader. The numbers on top denote vertical shifts between molecules. (b) Beta-sheets Sij, constructed by combining the Si and Sj patterns.

mission electron microscopy [QFDE-TEM, Fig. 3(b)], where the sample is frozen in solution, eliminating the effects of the probe tip or substrate.

B. Constructing β-sheets

The arrangement of strands in a β-sheet can be either parallel or anti-parallel. Preliminary simulations indicated that a parallel sheet of KFE8 molecules is less stable than the anti-parallel configuration due to an unfavorable electrostatic interaction between charged side chains, as explained in Sec. V A. Therefore we focused on anti-parallel β-sheets.

The extended conformation of KFE8 has an asymmetric distribution of backbone hydrogens and oxygens (Fig. 2). When a second molecule is placed anti-parallel to the first, there are two possible ways of arranging the hydrogen bonds. In Fig. 4(a), $S1$ and $S2$ are the possible hydrogen bonding patterns between the downward arrow and the one to its right. Similarly, $S3$ and $S4$ involve those to the left of the downward arrow. It is possible that larger shifts exist between peptides so that adjacent molecules share two or four hydrogen bonds, the overall β-sheet having a 'brick wall' structure.[31] However, this arrangement is more likely to yield a membrane than a thin helical ribbon, contradicting the observation in Fig. 3(a). Moreover, other researchers have reported that β-sheet peptides with various sequences form tapes a single molecule in width.[8,11,33] We therefore propose that the most probable hydrogen bonding patterns between two molecules are those in Fig. 4(a). The distance between two molecules was set to 4.77 Å, an average value from preliminary simulations of β-sheets built with these patterns. This agrees with the typical experimental value of 4.8 Å.[7,33] In order to construct the β-sheet Sij, we repeated patterns Si and Sj as in Fig. 4(b). Mixed patterns between these four are also possible, but are not likely to form regular helical ribbons.

C. Constructing the helix

Helical ribbons formed by KFE8 are left-handed. This is probably due to the right-handed twist along the backbone of a β-strand,[34] which forces two adjacent molecules to pack at an angle; construction of the helix followed this principle (Fig. 5). First we built a planar β-sheet in the yz plane, along the y axis, using one of the four configurations in Fig. 4(b). The sheet was then rotated around the x-axis to a given pitch angle θ, followed by successive rotation of the individual molecules around the z-direction. A more detailed description is given in the Appendix.

III. IONIZATION STATUS OF THE CHARGED SIDE CHAINS

Self-assembly of KFE8 is sensitive to pH and ionic strength of the solution due to ionizable side chains.[4,35] When the molecule carries zero net charge, or when the charges are screened, self-assembly of fibers occurs extremely rapidly. In order to slow down the process and to observe the intermediates, we dissolved the peptide in deionized water, which gave a pH of approximately 3 due to residual trifluoroacetic acid (TFA) from peptide synthesis. At this pH the molecules carry a net positive charge and self-assembly is slow. In order to incorporate this effect in our simulation, we needed to calculate the amount of charge on each side chain.

The pK values of Glu and Lys are, respectively, 4.3 and 10.8.[36] Plain dissociation kinetics would predict about 5% of Glu and 100% of Lys to be charged at pH 3. However, these side chains are spatially fixed and close to each other on the peptide backbone. For this reason, their behavior differs from that predicted by this theory.[37,38] To refine our calculation,

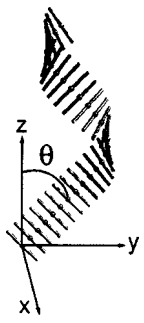

FIG. 5. The procedure of building a helical ribbon from a planar β-sheet.

we used the electrostatic double layer theory.[37,39] For simplicity, we assume that the β-sheet is an infinite plane immersed in water. In what follows, A and B, respectively, denote Glu and Lys, and all concentrations with subscript s are surface values.

The dissociation constants for AH and BH^+ can be expressed as

$$K_A=\frac{[A^-]_s[H^+]_s}{[AH]_s}, \quad K_B=\frac{[B]_s[H^+]_s}{[BH^+]_s}. \tag{1}$$

The maximum possible surface charge densities of A and B are given by

$$-\sigma_A^{max}=-eN_A, \quad \sigma_B^{max}=eN_B, \tag{2}$$

where $-e$ is the charge of an electron, and N_A and N_B are surface densities of side chains. We can then express the total surface charge density in partially ionized conditions as

$$\sigma=-\sigma_A^{max}\frac{[A^-]_s}{[AH]_s+[A^-]_s}+\sigma_B^{max}\frac{[BH^+]_s}{[BH^+]_s+[B]_s}. \tag{3}$$

The concentration $[H^+]_s$ can be expressed in terms of the bulk concentration $[H^+]_0$ using the Boltzmann relation

$$[H^+]_s=[H^+]_0e^{-e\psi_s/kT}, \tag{4}$$

where ψ_s is the electrostatic potential at the surface (the potential is set to zero at infinite separation from the surface), k is the Boltzmann constant and T is the temperature.

Substituting Eqs. (1) and (4) into Eq. (3) gives

$$\sigma=\frac{-\sigma_A^{max}K_A}{[H^+]_0\,e^{-e\psi_s/kT}+K_A}+\frac{\sigma_B^{max}[H^+]_0\,e^{-e\psi_s/kT}}{[H^+]_0e^{-e\psi_s/kT}+K_B}. \tag{5}$$

Here σ and ψ_s are the only unknowns. Another relation between σ and ψ_s can be obtained from the Grahame equation.[37] If there are n different ions in solution, with bulk concentrations c_i^0 $(i=1\cdots n)$ and valency z_i, the general form of the Grahame equation is[37]

$$\sigma^2=2\epsilon\epsilon_0kT\sum_i c_i^0(e^{-z_ie\psi_s/kT}-1), \tag{6}$$

where ϵ is the dielectric constant of water ($\sim$80) and ϵ_0 is the permittivity of vacuum. Equations (5) and (6) can be numerically solved to give σ and ψ_s. Charged fractions of A and B can be obtained from the two terms on the right-hand side of Eq. (5).

To better understand the pH dependence of our system, we performed a thought titration experiment where a monovalent base D is added to the solution. The maximum surface charge densities can be calculated from the dimensions of KFE8 (Fig. 2) as $\sigma_{Glu}^{max}=\sigma_{Lys}^{max}\simeq 0.22$ C/m^2. Denoting $[T^-]$ as the concentration of the residual TFA, the relevant concentrations in Eq. (6) are $[T^-]_0$, $[D^+]_0$, $[H^+]_0$, and $[OH^-]_0$, where the subscript 0 refers to bulk concentrations. Substituting the charge neutrality condition $[D^+]_0=[T^-]_0-[H^+]_0+[OH^-]_0$ into Eq. (6), one obtains

$$\sigma=\sqrt{8\epsilon\epsilon_0kT([OH^-]_0+[T^-]_0)}\,\sinh\left(\frac{e\psi_s}{2kT}\right). \tag{7}$$

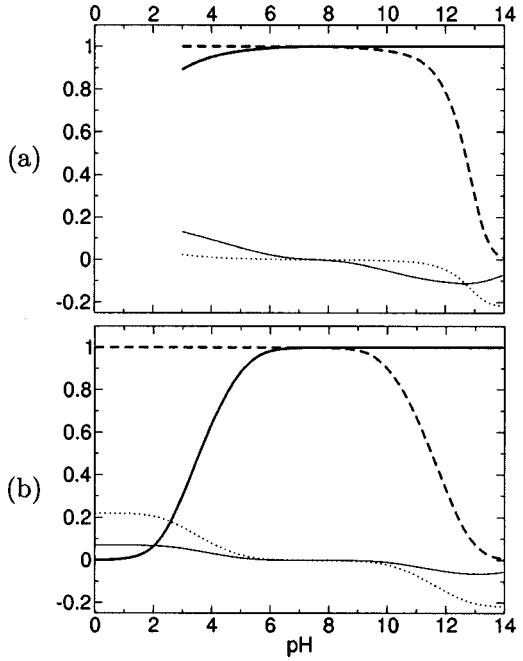

FIG. 6. Titration curves of the infinite planar β-sheet with Glu and Lys side chains. The titration starts from (a) pH 3.0 and (b) pH 0.0. Thick solid line: fraction of negatively charged Glu; thick dashed: fraction of positively charged Lys; dotted: total surface charge density σ(C/m^2); thin solid line: surface electrostatic potential ψ_s (Volts).

With $[T^-]_0$ fixed and $[OH^-]_0=10^{pH-14}$, the titration curve can be obtained by solving Eqs. (5) and (7) numerically. The result depends on the titration history, as shown by the two following scenarios. First, the initial pH of the solution is set to 3, as in our experiments, and $[T^-]_0=10^{-3}$. In the second scenario, we start the titration from pH 0 (Fig. 6). At pH 3 Lys is fully charged, while the fraction of charged Glu varies between 0.30 (second scenario) and 0.89 (first scenario). The ''apparent'' pK_E, defined as the value of pH where half of Glu are charged, varies according to the titration history as well. For example, in Fig. 6(b), pK_E is 3.59, instead of 4.3. It is interesting to note that this falls within the range 3.23–3.87 calculated by Monte Carlo simulations.[38]

IV. SIMULATION METHODS

We used CHARMM[40] with polar hydrogen parameter set param19. As the system is in an aqueous solution, it is important to include the solvation effect in the simulation. Since modeling explicit water molecules would be computationally prohibitive, we used the analytic continuum electrostatics (ACE) model[41,42] incorporated into CHARMM. The ACE model works well in describing the solvation effect of small systems, except where the explicit geometry of water molecules is critical (such as near an enzyme binding site or for proteins with complex topology).[42] In the case of our helical ribbons, charged side chains are distributed on smoothly curved surfaces and we expect the effect of water molecules to be mostly thermodynamic. Therefore ACE should be a reasonably good approximation of solvation and hydrophobic interactions in our system.

FIG. 7. A segment of the double β-sheet helix used in simulations. Arrows represent peptides in β-strand conformation (Ref. 45). (a) Side view; (b) axial view.

We started our simulation with a helical ribbon composed of a single β-sheet (Fig. 5). This structure was found to be unstable, collapsing immediately, since hydrophobic side chains on the inner side are still exposed to water. Thus we concentrated on double sheet helices, consistent with the measured dimensions from the AFM image (Sec. II A).

Since there are four possible β-sheets for each of the inner and outer layers, 16 different helices can be built. We constructed the outer helix according to the experimental dimensions, while the inner helix was built to contact the outer one from the inside. The backbone distance between the two layers was 12.9 Å. Each simulation was performed on a helical segment composed of 40 molecules (Fig. 7). To investigate the effect of the system size, we also ran simulations with 60 peptides in some cases. These are less than one turn of a helix, which contains 77–99 peptides depending on the particular β-sheet combination [Eq. (A3)].

The effect of pH was incorporated by scaling the charge on each ionizable side chain by the method explained in Sec. III, an idea originally used in vacuum simulation to mimic the effect of bulk solvent.[43] From Fig. 6(a), we left the Lys fully charged and the Glu 90% charged for pH 3. The dependence on charge scaling will be presented in Sec. V C.

After the structure was built, the MD followed these steps: an initial energy minimization procedure of 400 steps with the steepest descent method, followed by 2000 steps of the adapted basis Newton–Raphson method. Then the system was heated from 98 K to 298 K for 30 ps and equilibrated for 30 ps. The production run lasts for 40 ps where the coordinate trajectories were averaged and energy minimized once again. The time step of the simulation was 1 fs. Simulation on each helical ribbon took about 8 hours on a custom built Beowulf cluster with ten 1.7 GHz CPUs (Intel Xeon) connected via an optical gigabit network.

V. RESULTS AND DISCUSSION

We first identified the most stable supramolecular packing by running MD on each of the 16 helices. Although the helices were constructed using the experimentally measured dimensions, the selection of the most stable packing pattern is independent of the helical geometry. Then we systematically varied the geometry of the helix with the most stable packing pattern to explore its energy landscape, and found a local energy minimum at the experimentally measured pitch and pitch angle. Finally we investigated the dependence of our results on charge scaling. Only the simulation with the charge scaling corresponding to the experimental pH gave consistent results with the experiment.

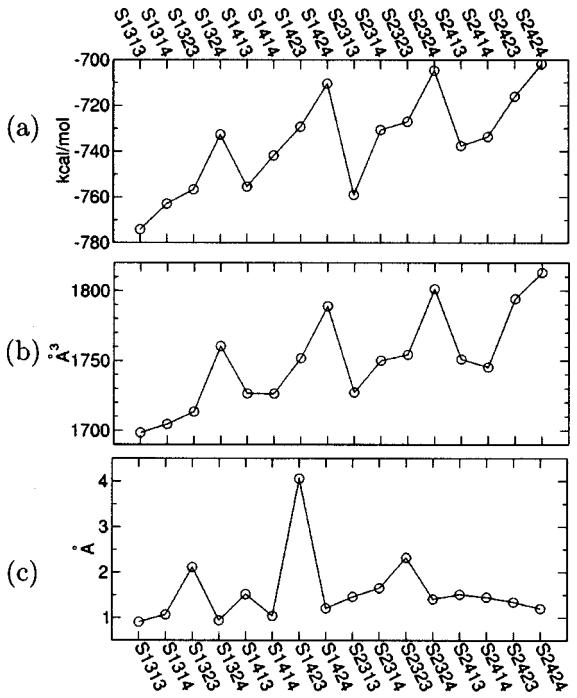

FIG. 8. An analysis of structures in Fig. 9. (a) Energy and (b) volume per peptide, (c) average RMS fluctuation per atom. A horizontal axis denotes helices built by different combinations of β-sheets.

In comparing the stability of different structures, minimization of the energy per molecule is the most important criterion. This includes both the intra- and the intermolecular energies, as well as the solvation free energy. We also used the minimization of volume per molecule and root mean square (RMS) fluctuation per atom as auxiliary criteria, expecting tight molecular packing and small fluctuations to be associated with a stable structure.

A. Supramolecular packing

The comparison between different packing geometries is summarized in Fig. 8. Here $Sijkl$ denotes a double sheet helix where the Sij and Skl sheets are, respectively, used for the inner and the outer helices. Our results suggest that the $S1313$ is the most probable supramolecular packing for the helical ribbon. The energy difference between the $S1313$ and the next lowest one, $S1314$ is 11.2 kcal/mol, sufficiently larger than $kT \simeq 0.6$ kcal/mol. Figure 9 shows the minimized structures after simulation. Compared to the initial shape (Fig. 7), some of them are severely distorted [for example, the $S1423$, consistent with Fig. 8(c)].

We also ran simulations with 60 peptides for the helices with the five lowest energies in Fig. 8 ($S1313$, $S1314$, $S1323$, $S1413$ and $S2313$). The $S1313$ still had the lowest energy (data not shown). Moreover, the energy difference between the $S1313$ and the others increased. For example, the $S1314$ (the next lowest in energy) had energy per peptide higher than the $S1313$ by 11.2 kcal/mol (40 peptides) and 14.5 kcal/mol (60 peptides).

This result can be explained by the electrostatic interaction between charged side chains, as the Debye length is about 10 nm at pH 3 ($\sim$1 mM electrolyte concentration), several times larger than the distance between neighboring

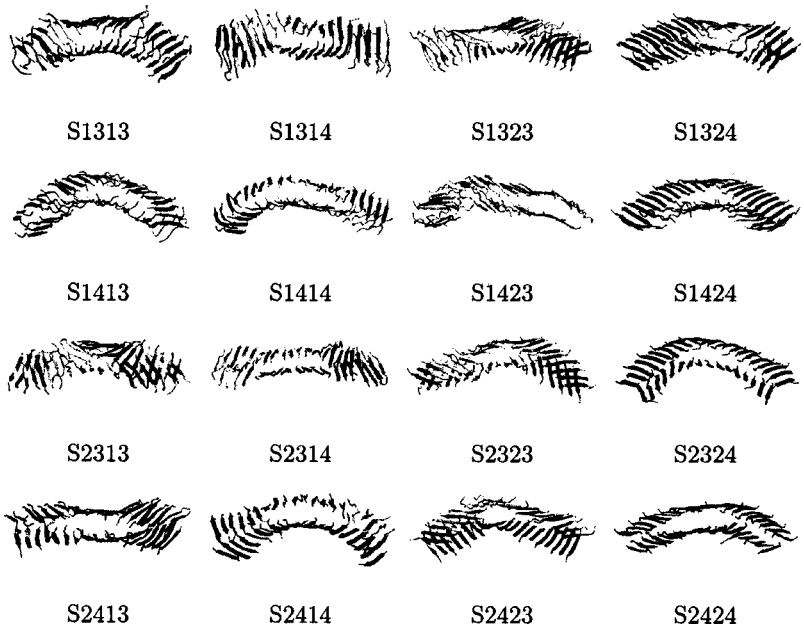

FIG. 9. Side views of the 16 different helices after the MD.

side chains. The $S1$ and $S3$ patterns (Fig. 10) are energetically favorable, as oppositely charged side chains are adjacent to each other, while less favorable situations occur in other cases. For example, the $S2424$ helix has the highest energy because equal charges are next to each other. As mentioned in Sec. II B, a parallel β-sheet is unfavorable for the same reason. Since this argument does not assume a particular helical geometry, our result is expected to hold independent of the detailed conformation of the helix.

It is somewhat surprising that a system comprised of two identical β-sheet tapes can form into a two-layer helical ribbon since, in that conformation, the inner and outer tapes have different curvatures. According to Aggeli *et al.*,[30] such systems comprised of identical tapes are more likely to twist around a fixed axis, exhibiting a saddle-point curvature, rather than form a helical structure. In our system, however, the two sheets share only the backbone hydrogen bonding pattern, so that the flexible side chains on the inner and outer helices can reside in different conformations, thereby establishing a natural asymmetry. Other examples of symmetry breaking of this type can be found in certain lipid bilayers that can undergo transitions between twisted ribbons and helices.[20,44] Thus, while currently available evidence points to the helical structure $S1313$, the mechanism of curvature selection in general, and in this specific instance, as well, remains an open question. These issues are discussed in greater depth in Selinger *et al.*[44]

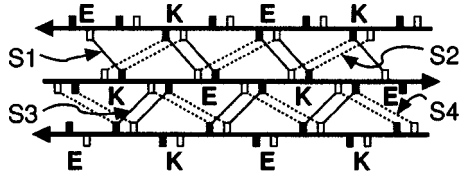

FIG. 10. Locations of charged side chains in each hydrogen bonding pattern. The Phe side chains are out of the page, as in Fig. 4(a). Backbone hydrogens and oxygens are denoted as hollow and solid boxes, respectively. The patterns $S1$, $S3$ are solid, and $S2$, $S4$ are denoted as dashed lines. To obtain a desired β-sheet, neighboring strands should be shifted horizontally by the amount in Fig. 4(a).

B. Energy landscape of the helical ribbon

We next varied the geometry of the $S1313$ helix to investigate its energy landscape. In order to limit computational time we searched the phase space only along two orthogonal lines: we first fixed the pitch angle and varied the pitch; then we did the reverse. The range of values tested was comparable to the one found in the experiments. In order to investigate the deformation of a *given* helix, we also varied both quantities while keeping the contour length per helical turn fixed.

Figure 11 shows the result for the case when the pitch is varied while the pitch angle is fixed. There are several local energy minima at different pitches. The stability of these minima can be considered by comparing their depth with kT. In the 40-peptide simulation, there are three major minima at 16, 19 and 25 nm pitches. However, only the minimum at 19 nm does not change its location in the simulation with 60 peptides. Thus the other minima are likely to come from the finite system size, which is less than half a helical turn. In particular, the lowest minimum changed its location from 25 nm (40 peptides) to 14 nm (60 peptides). The helix with 14 nm pitch may be regarded as a ''rotated'' view of a helix with an even lower pitch and a larger pitch angle, possibly indicative of the more stable fibrous structure observed later in the self-assembly. Such an ambiguity is expected to decrease as the system size gets larger.

Note also that the overall energy level has decreased in the 60-peptide simulation. This is a general tendency which reflects the lowering of the energy per peptide for a larger cluster size, a necessary condition for self-assembly.[37]

Next, we vary the pitch angle with the pitch fixed at 19 nm, as shown in Fig. 12. The minimum at 41° agrees well

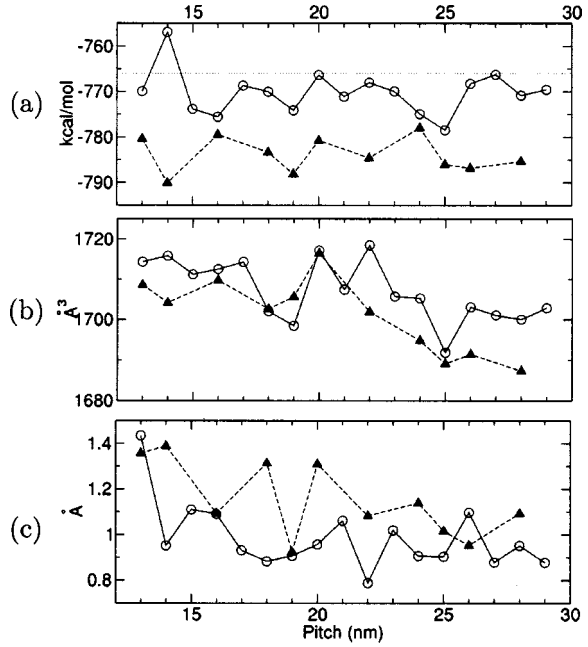

FIG. 11. Pitch dependence of the *S*1313 helix, with the pitch angle fixed at 41°. (a) Energy and (b) volume per peptide, (c) average RMS fluctuation per atom. Open circle: 40-peptide, filled triangle: 60-peptide simulations. The dotted line in (a) denotes the energy in the case of a 40-peptide, planar *S*1313 sheet.

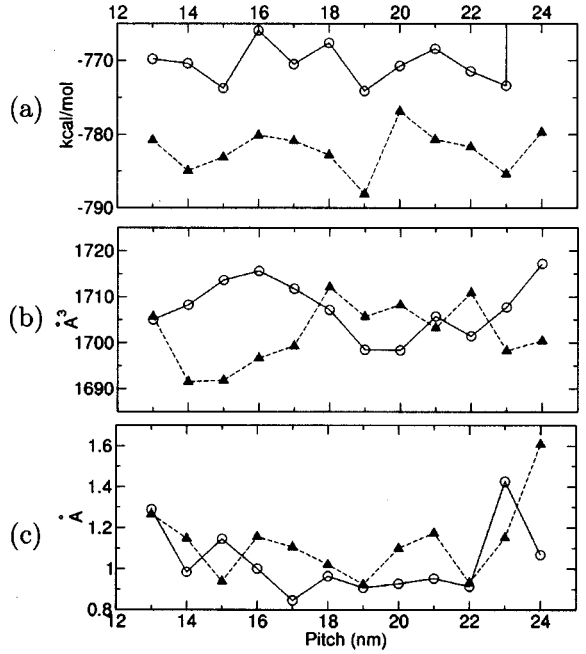

FIG. 13. Deformation of the *S*1313 helix with a fixed contour length per helical turn. The reference pitch and pitch angle are 19 nm and 41°. (a) Energy and (b) volume per peptide; (c) average RMS fluctuation per atom. Open circle: 40-peptide, filled triangle: 60-peptide simulations. The energy at 24 nm pitch of the 40-peptide simulation is -174 kcal/mol.

with the experiments. Compared to Fig. 11, there is only one major minimum because the change in curvature is less than in the previous case. The helices corresponding to the angular range 35°–49° have 90 to 110 peptides per helical turn, while in the previous case of pitch variation, the number varies from 64 (13 nm pitch) to 151 (29 nm pitch). Indeed, the portion of Fig. 11(a) between 18 nm and 22 nm is similarly smooth as Fig. 12(a), where the number of molecules per turn varies between 91 and 113. From these, we have found that the energy landscape of the system has a well-defined local minimum at the 19 nm pitch and the 41° pitch angle, consistent with experiments.

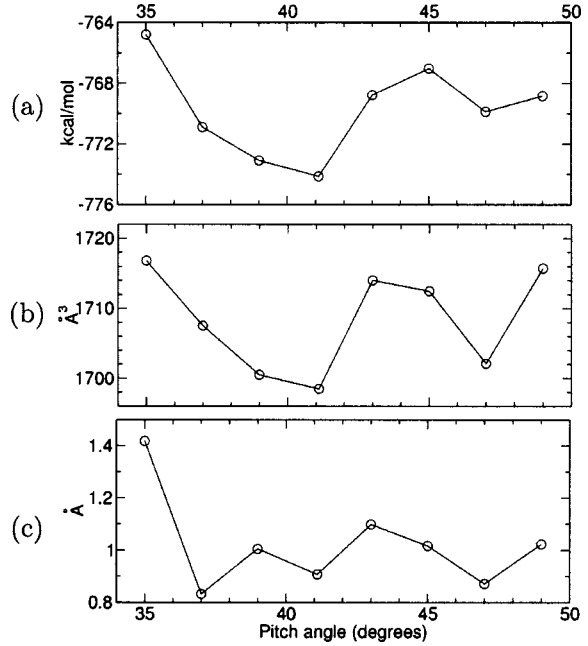

FIG. 12. Pitch angle dependence of the *S*1313 helix with pitch fixed at 19 nm. Simulations run with 40 peptides. (a) Energy and (b) volume per peptide; (c) average RMS fluctuation per atom.

Finally, we show the result for the case with a fixed contour length per helical turn in Fig. 13. Due to this constraint, the pitch cannot go beyond 24 nm, as can be seen by the sharp increase either in energy (40-peptide simulation) or in the RMS fluctuation (60-peptide simulation). High RMS fluctuations at large pitches are indicative of rapid relaxation of the system due to stretch-induced stress. Again in good agreement with the experiments, the pitch at 19 nm is the most stable. Similar to Fig. 11(a), this minimum alone does not change its location with different system sizes. The range of pitches whose energy is larger than the minimum at 19 nm by kT is on the order of 1 nm, also consistent with the standard deviation of the experimental measurement, 1.3 nm.

C. Effect of charge scaling

In the previous sections we have scaled the charge on Glu by 90% to simulate the condition of *p*H 3. Here we investigate the sensitivity of our results to charge scaling by applying 60% and 100% charge on Glu. From the calculations in Sec. III, these two situations correspond, respectively, to *p*H 2.1 and 7. We varied the pitch while keeping the contour length fixed, and the results are shown in Figs. 14. The 19 nm pitch is clearly not a minimum anymore, suggesting the importance of charge scaling.

Experimentally, we have observed helical ribbons even at *p*H 1.5, but not at *p*H 7. As the simulations are based on the experimental geometry found in *p*H 3, we expect the data

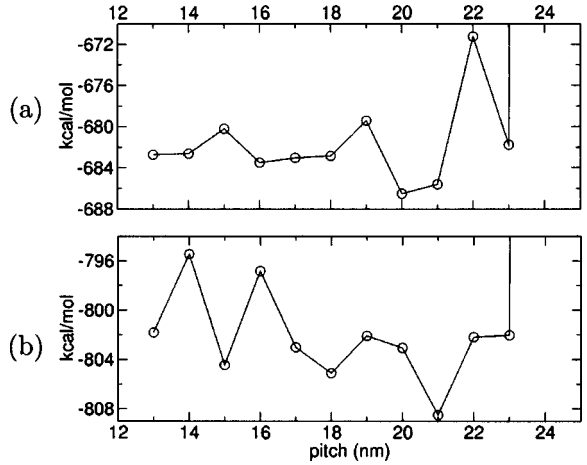

FIG. 14. Dependence on charge scaling, with fixed contour length per helical turn. The energy per peptide of the *S*1313 helix (40 peptides) with Glu (a) 60%, (b) 100% charged. The energy at 24 nm is (a) −85.7 kcal/mol and (b) −214 kcal/mol.

with 60% scaling to be closer to the real situation than that with 100% scaling. According to Fig. 14(a), the system may have a longer pitch at a lower *p*H. However, the accuracy of charge scaling decreases with greater charge reduction as it is a static approximation of the dynamic protonation process. More experiments need be performed to test the dependence of the pitch on *p*H.

VI. CONCLUSION

We have developed a computational method to identify the most probable supramolecular structure and properties of the helical ribbon intermediates formed during self-assembly of KFE8. Our results suggest that these helical ribbons are composed of a double β-sheet where the inner and the outer helices have the same (*S*13) hydrogen bonding pattern. The mechanism by which the system selects the helical curvature is not yet clear. The number of molecules per helical turn is about 100 (44 for the inner, 53 for the outer helix). Electrostatic interactions between charged side chains were found to be crucial in determining the hydrogen bonding pattern and geometry of the helix. Systematic variation of the helical geometry was performed to explore its energy landscape, and we have found a local energy minimum consistent with the experimentally measured pitch and pitch angle.

Because the hydrogen bonding pattern is determined by the side chain interactions, not by the helical geometry, we expect the fibers observed at later times during the self-assembly of KFE8 to have the same packing as the helical ribbon intermediates. Therefore it is possible to extend our method to study the helix to fiber transition by making a helix with tighter pitch and following its dynamics. The elastic properties of the fiber can be measured similarly by applying deformations in relevant directions. Such quantitative information can be used for developing a continuum description of the system.

Our computational approach is a complementary tool to experimental observations. With the increase of computational power, it will be possible to sample a large number of peptide sequences to design novel biomaterials with prescribed properties *in silico*, rather than trying out each design experimentally. Such an approach may also provide a better understanding of the structure and the formation of amyloid fibrils.

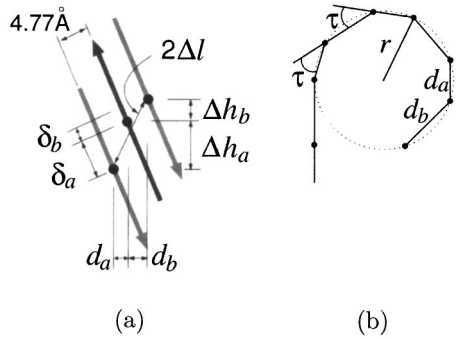

FIG. 15. The procedure of building a helical ribbon. (a) Relevant lengths in the planar β-sheet slanted to the pitch angle. The dot in the middle of a strand denotes the center of mass. (b) The view of Fig. 5 through the *z*-axis.

ACKNOWLEDGMENTS

We thank B. Tidor, B. Sherman, M. Altman, and A. Keating for helpful discussions on computational methods. This work is funded by the DuPont–MIT Alliance. We gratefully acknowledge the generous donation of computers by the Intel Corporation.

APPENDIX A: PROCEDURE OF BUILDING A HELIX

A helix can be constructed from a planar β-sheet first by rotating the sheet to a certain pitch angle and then folding the sheet along the *z*-direction at points where the centers of mass of the molecules are located (Fig. 5). Figure 15(a) shows relevant lengths after the β-sheet is rotated to the pitch angle. Here, Δl is the average center of mass distance between the molecules, and δ_a, δ_b are relative shifts between peptides along the strand [Fig. 4(a)]. The view of Fig. 5 along the *z*-axis is in Fig. 15(b).

Experimentally, the pitch h and the pitch angle θ of a helix are measurable quantities, and its radius r can be found by the relation

$$r = \frac{h}{2\pi} \tan \theta. \tag{A1}$$

However, this is only an approximate expression due to the discrete nature of the system; the lengths d_a, d_b are shorter than the arc length on the circle in Fig. 15(b). Especially when building a double sheet helix, the pitch angle of the inner helix cannot be measured. While the inner radius r_i is determined based on the outer radius (Sec. IV), the inner pitch angle calculated by using this r_i in Eq. (A1) gives rise to a mismatch between the inner and the outer sheets. Thus we use the pitch and the radius as control parameters when building the helix. Equation (A1) is used only when initially obtaining the outer radius from measured h and θ. The prob-

lem then becomes one of identifying the pitch angle θ and the folding angle τ [Fig. 15(b)] for given pitch and radius of the helix.

It can be shown that the values of θ and τ obtained by uniformly shifting the peptides by $\delta=(\delta_a+\delta_b)/2$ are the same as those when $\delta_a \neq \delta_b$. We further define other averages $d=(d_a+d_b)/2$, $\Delta h=(\Delta h_a+\Delta h_b)/2$, and $\Delta l=\{\delta^2+(4.77\ \text{Å})^2\}^{1/2}=\sqrt{\Delta h^2+d^2}$. Using these, we get

$$h=N\Delta h, \quad d=2r\sin\left(\frac{\pi}{N}\right), \tag{A2}$$

where N is the number of peptides per helical turn. We insert Δh and d into the relation $\Delta l^2=\Delta h^2+d^2$ to get

$$\Delta l^2=\frac{h^2}{N^2}+4r^2\sin^2\left(\frac{\pi}{N}\right). \tag{A3}$$

For given values of h, r and Δl, we can calculate N by numerically solving Eq. (A3). Using Eq. (A2), we then get $\Delta h=h/N$, and from Fig. 15,

$$\theta=\cos^{-}\left(\frac{\Delta h}{\Delta l}\right), \quad \tau=\frac{2\pi}{N}. \tag{A4}$$

Equation (A4) specifies the necessary transformation to build the helical ribbon. The helical ribbon is left-handed with hydrophobic side chains on the inside of the helix. To build an inner helix which has the hydrophobic side chains on its outer side, we simply replace $\theta\rightarrow\pi-\theta$ and $\tau\rightarrow-\tau$.

[1] S. Zhang, T. Holmes, C. Lockshin, and A. Rich, Proc. Natl. Acad. Sci. U.S.A. **90**, 3334 (1993).
[2] T. C. Holmes, S. de Lacalle, X. Su, G. Liu, A. Rich, and S. Zhang, Proc. Natl. Acad. Sci. U.S.A. **97**, 6728 (2000).
[3] D. M. Marini, W. Hwang, D. A. Lauffenburger, S. Zhang, and R. D. Kamm, Nano Letters **2**, 295 (2002).
[4] M. R. Caplan, P. N. Moor, S. Zhang, R. D. Kamm, and D. A. Lauffenburger, Biomacromolecules **1**, 627 (2000).
[5] A. Aggeli, M. Bell, N. Boden, J. N. Keen, P. F. Knowles, T. C. B. McLeish, M. Pitkeathly, and S. E. Radford, Nature (London) **386**, 259 (1997).
[6] J. D. Kisiday, M. Jin, B. Kurz, H. Huang, C. E. Semino, S. Zhang, and A. J. Grodzinsky, Proc. Natl. Acad. Sci. U.S.A. **99**, 9996 (2002).
[7] M. Balbirnie, R. Grothe, and D. S. Eisenberg, Proc. Natl. Acad. Sci. U.S.A. **98**, 2375 (2001).
[8] T. Kowalewski and D. M. Holtzman, Proc. Natl. Acad. Sci. U.S.A. **96**, 3688 (1999).
[9] N. D. Lazo and D. T. Downing, Biochem. Biophys. Res. Commun. **235**, 675 (1997).
[10] J. J. Balbach, Y. Ishii, O. N. Antzukin, R. D. Leapman, N. W. Rizzo, F. Dyda, J. Reed, and R. Tycko, Biochemistry **39**, 13748 (2000).
[11] T. S. Burkoth, T. L. S. Benzinger, V. Urban, D. M. Morgan, D. M. Gregory, P. Thiyagarajan, R. E. Botto, S. C. Meredith, and D. G. Lynn, J. Am. Chem. Soc. **122**, 7883 (2000).
[12] T. L. S. Benzinger, D. M. Gregory, T. S. Burkoth, H. Miller-Auer, D. G. Lynn, R. E. Botto, and S. C. Meredith, Biochemistry **39**, 3491 (2000).
[13] T. L. S. Benzinger, D. M. Gregory, T. S. Burkoth, H. Miller-Auer, D. G. Lynn, R. E. Botto, and S. C. Meredith, Proc. Natl. Acad. Sci. U.S.A. **95**, 13407 (1998).
[14] O. N. Antzutkin, J. J. Balbach, R. D. Leapman, N. W. Rizzo, J. Reed, and R. Tycko, Proc. Natl. Acad. Sci. U.S.A. **97**, 13405 (2000).
[15] G. F. Egnaczyk, K. D. Greis, E. R. Stimson, and J. E. Maggio, Biochemistry **40**, 11706 (2001).
[16] J. D. Harper, S. S. Wong, C. M. Lieber, and P. T. Lansbury, Biochemistry **38**, 8972 (1999).
[17] K. A. Conway, S.-J. Lee, J.-C. Rochet, T. T. Ding, R. E. Williamson, and P. T. Lansbury, Proc. Natl. Acad. Sci. U.S.A. **97**, 571 (2000).
[18] M. P. Lambert, A. K. Barlow, B. A. Chromy *et al.*, Proc. Natl. Acad. Sci. U.S.A. **95**, 6448 (1998).
[19] M. J. Volles, S.-J. Lee, J.-C. Rochet, M. D. Shtilerman, T. T. Ding, J. C. Kessler, and P. T. Lansbury, Biochemistry **40**, 7812 (2001).
[20] R. Oda, I. Huc, M. Schmutz, S. J. Candau, and F. C. MacKintosh, Nature (London) **399**, 566 (1999).
[21] B. N. Thomas, C. M. Lindemann, and N. A. Clark, Phys. Rev. E **59**, 3040 (1999).
[22] B. Smith, Y. V. Zastavker, and G. B. Benedek, Phys. Rev. Lett. **87**, 278101 (2001).
[23] M. S. Spector, A. Singh, P. B. Messersmith, and J. M. Schnur, Nano Letters **1**, 375 (2001).
[24] E. Rogalska, M. Rogalski, T. Gulik-Krzywicki, A. Gulik, and C. Chipot, Proc. Natl. Acad. Sci. U.S.A. **96**, 6577 (1999).
[25] T. Gulik-Krzywicki, C. Fouquey, and J.-M. Lehn, Proc. Natl. Acad. Sci. U.S.A. **90**, 163 (1993).
[26] H. Engelkamp, S. Middelbeek, and R. J. M. Nolte, Science **284**, 785 (1999).
[27] I. A. Nyrkova, A. N. Semenov, A. Aggeli, and N. Boden, Eur. Phys. J. B **17**, 481 (2000).
[28] I. A. Nyrkova, A. N. Semenov, A. Aggeli, M. Bell, and T. C. B. M. N. Boden, Eur. Phys. J. B **17**, 499 (2000).
[29] J. V. Selinger, F. C. MacKintosh, and J. M. Schnur, Phys. Rev. E **53**, 3804 (1996).
[30] A. Aggeli, I. A. Nyrkova, M. Bell, R. Harding, L. Carrick, T. C. B. McLeish, A. N. Semenov, and N. Boden, Proc. Natl. Acad. Sci. U.S.A. **98**, 11857 (2001).
[31] S. Zhang, C. Lockshin, R. Cook, and A. Rich, Biopolymers **34**, 663 (1994).
[32] M. Altman, P. Lee, A. Rich, and S. Zhang, Protein Sci. **9**, 1095 (2000).
[33] A. Aggeli, M. Bell, N. Boden, J. N. Keen, T. C. B. McLeish, I. Nyrkova, S. E. Radford, and A. Semenov, J. Mater. Chem. **7**, 1135 (1997).
[34] I. L. Shamovsky, G. M. Ross, and R. J. Riopelle, J. Phys. Chem. B **104**, 11296 (2000).
[35] M. R. Caplan, Ph.D. thesis, Massachusetts Institute of Technology, 2001.
[36] L. Stryer, *Biochemistry*, 4th ed. (W. H. Freeman and Company, New York, 2000).
[37] J. Israelachvili, *Intermolecular and Surface Forces*, 2nd ed. (Academic, London, 1992).
[38] P. J. Kundrotas and A. Krashikoff, Phys. Rev. E **65**, 011901 (2001).
[39] T. W. Healy and L. R. White, Adv. Colloid Interface Sci. **9**, 303 (1978).
[40] B. R. Brooks, R. E. Bruccoleri, B. D. Olafson, D. J. States, S. Swaminathan, and M. Karplus, J. Comput. Chem. **4**, 187 (1983).
[41] M. Schaefer and M. Karplus, J. Phys. Chem. **100**, 1578 (1996).
[42] M. Schaefer, C. Bartels, and M. Karplus, J. Mol. Biol. **284**, 835 (1998).
[43] T. Simonson, G. Archontis, and M. Karplus, J. Phys. Chem. **101**, 8349 (1997).
[44] J. V. Selinger, M. S. Spector, and J. M. Schnur, J. Phys. Chem. B **105**, 7157 (2001).
[45] W. Humphrey, A. Dalke, and K. Schulten, J. Mol. Graphics **14**, 33 (1996).